Electronic Biosensing with Flexible Organic Transistor Devices

Caroline Kotlowski, Patrik Aspermair, Hadayat Ullah Khan, Ciril Reiner-Rozman, Josef Breu, Sabine Szunerits, Jang-Joo Kim, Zhenan Bao, Christoph Kleber, Paolo Pelosi, et al.

Flexible and Printed Electronics

Electronic biosensing with flexible organic transistor devices

Flexible and Printed Electronics

PAPER

Electronic biosensing with flexible organic transistor devices

Caroline Kotlowski[1,2], Patrik Aspermair[1,2,3], Hadayat Ullah Khan[4], Ciril Reiner-Rozman[1,2], Josef Breu[5], Sabine Szunerits[3], Jang-Joo Kim[6], Zhenan Bao[7], Christoph Kleber[1], Paolo Pelosi[2] and Wolfgang Knoll[1,2]

[1] Center for Electrochemical Surface Technology (CEST), Wiener Neustadt, Austria
[2] AIT Austrian Institute of Technology, Tulln, Austria
[3] Université de Lille, France
[4] Fingerprint Cards AB, Kungsgatan 20, 41119 Goteborg, Sweden
[5] Inorganic Chemistry I, University of Bayreuth, Bayreuth, Germany
[6] Department of Materials Science and Engineering, Seoul National University, Seoul, Republic of Korea
[7] Department of Chemical Engineering, Stanford University, CA, United States of America

E-mail: wolfgang.knoll@ait.ac.at

Keywords: electronic biosensing, immunosensing, antigen–antibody interaction, OFET, rGO–FET, biomimetic smell sensing

OPEN ACCESS

RECEIVED
4 May 2018

REVISED
19 June 2018

ACCEPTED FOR PUBLICATION
18 July 2018

PUBLISHED
7 September 2018

Abstract

In this short review, we summarize the design and implementation of organic semiconducting materials-based field-effect transistors (OFETs) and the fabrication and use of reduced graphene-oxide field-effect transistors (rGO–FETs) as flexible transducers for electronic biosensing. We demonstrate that these platforms allow for the quantitative, *in situ*, and in real time monitoring of bio-affinity reactions between analytes from solution to the surface-immobilized receptors. The examples given include the binding of anti-bovine serum albumin (BSA) antibodies to their antigen, BSA, covalently attached to the channel of an OFET, or the reverse mode of operation, i.e., the binding of BSA from solution to the antibodies immobilized on a rGO transistor. Finally, we will discuss a few results obtained with odorant binding proteins used as receptors on a rGO–FET transducer for the realization of a biomimetic smell sensor.

Introduction

Recently, the field of organic electronics has attracted increasing interest and a consequent growth in scientific research [1, 2]. A particular focus has been on wearable electronics for sensing and monitoring applications [3–5]. Current wearable sensors monitor simple analytes, such as ions, glucose, lactate, etc. In contrast, the human body emits hundreds of volatile organic compounds (VOCs), indicators of a person's health status, their metabolic activity, or their stress situation.

Electronic smell sensors are best suited for such applications as they (i) can be integrated into cell phones for breath analysis [6, 7], (ii) can be embedded into the fabric of clothing to monitor physiological and pathological conditions [8], and (iii) they could also be even implanted into the body for continuous monitoring of specific markers [9].

In addition to the category of flexible organic electrochemical transistors that have gained interest [10], electronic field-effect transistor (FET-) sensing devices can be:

- based on organic semiconducting materials (defined as an organic field-effect transistor (OFET)) [11–13];
- made on flexible and stretchable substrates [14, 15];
- fabricated on graphene [16];
- functionalized by biomimetic molecular modules like antibodies [17, 18], oligonucleotide capture strands [19], aptamers for marker molecules [20] and small VOCs [21], or odorant binding proteins to monitor olfactory cues [22];
- operated in liquids [11] and in air (provided the sensitive biological material is protected by hydrogels) [23].

In this paper, we summarize some of our own research results in this area. The first example that we discuss concerns the design and assembly of a flexible OFET and its characterization as an electronic transducer for the quantitative evaluation of the recognition reaction between a model marker protein, bovine serum albumin (BSA), immobilized on the channel

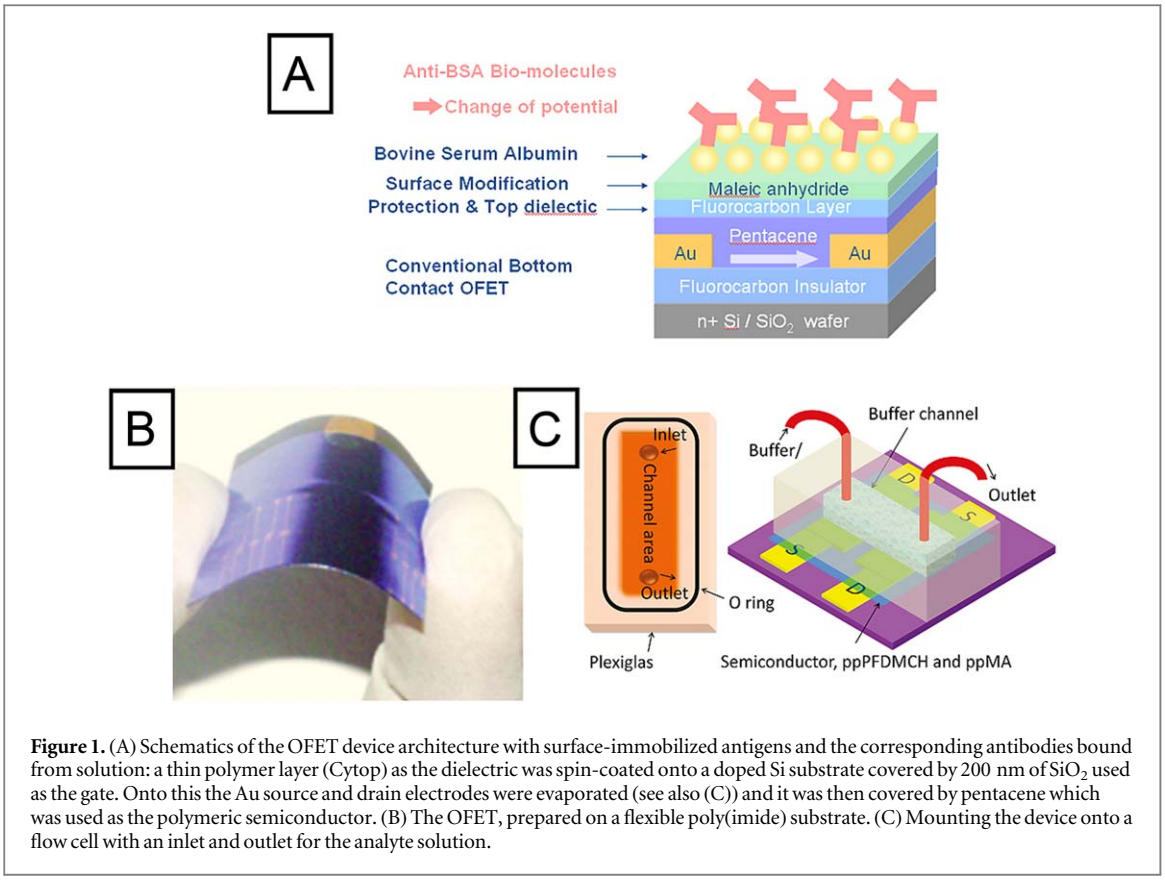

Figure 1. (A) Schematics of the OFET device architecture with surface-immobilized antigens and the corresponding antibodies bound from solution: a thin polymer layer (Cytop) as the dielectric was spin-coated onto a doped Si substrate covered by 200 nm of SiO_2 used as the gate. Onto this the Au source and drain electrodes were evaporated (see also (C)) and it was then covered by pentacene which was used as the polymeric semiconductor. (B) The OFET, prepared on a flexible poly(imide) substrate. (C) Mounting the device onto a flow cell with an inlet and outlet for the analyte solution.

surface of the transistor, and a high affinity antibody binding from solution.

In the next section, we then introduce a novel material, graphene, as the channel material connecting the source and drain electrodes of a transistor. As a test sample, we again use the BSA–anti-BSA antibody system; this time, however, we immobilized the antibody on the gate surface and characterized the performance of the device as an electronic sensor monitoring the binding of the analyte, BSA, from solution.

And finally, we present a few results of a major effort in our group, i.e., the use of graphene-based FET devices as electronic biomimetic smell sensors.

Protein (antibody) sensing by OFET devices

The use of Si-based electronic devices for monitoring biological processes is relatively well established [24, 25]. What has been less demonstrated so far is the use of organic electronic devices, which appear much more recently in the literature, as an option to be applied in combination with physiological buffer solutions for biosensing applications [26].

Our approach was based on a design concept given in figure 1: a very thin layer of a fluoro-polymer, Cytop, as the dielectric, was applied by spin-coating onto a 200 nm thin SiO_2 coating plus the Si substrate, which was highly doped in order to be used as the back-side gate electrode of the transistor. After evaporating the source and the drain Au electrodes (with a width (W) of 500 μm and length (L) of 50 μm), pentacene, as the semiconducting organic material, was deposited by evaporation [14] (figure 1(A)). Alternatively, a flexible poly(imide) substrate could be used for the device fabrication, resulting in a transistor that could be easily bend (figure 1(B)) [14].

An ultrathin (5–10 nm) fluorocarbon layer functioning as a protective barrier that prevents ions from the adjacent analyte buffer solution from diffusing into the organic channel material was deposited onto this OFET device by plasma polymerization. This is also shown schematically in figure 1(A). The further (vacuum) deposition of a maleic anhydride layer then allows for the direct coupling of biological functional units to the device structure via their amine moieties, e.g., the lysine groups of proteins. These then act as receptors for bio-affinity reactions between these surface-immobilized units and their interaction partners, the analytes of interest. This is depicted in figure 1(A) for the immobilization of BSA, with its antibody as the analyte, binding from solution. These transistor devices were then mounted to a flow cell and exposed to analyte solutions of different concentrations for binding studies *in situ* and in real time (figure 1(C)).

An example for a global analysis, i.e., the combination of kinetic and titration measurements for anti-BSA binding to surface-immobilized BSA proteins, is shown in figure 2. Upon injecting analyte solutions of increasing concentrations, c, a decreasing current between the source and the drain is seen, reflecting the

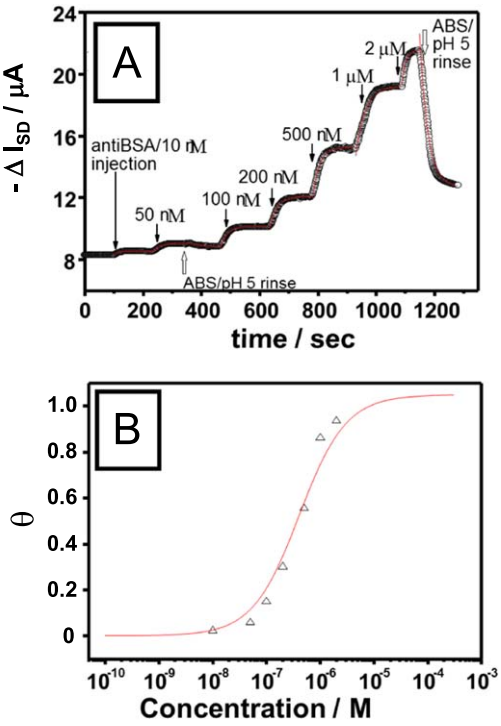

Figure 2. (A) Global analysis of the binding of anti-BSA antibodies from solutions of increasing concentrations to the surface-immobilized antigen molecules, BSA; (B) Langmuir adsorption isotherm from the titration date of (A), plotted as surface coverage, θ, as a function of the concentration of BSA in the bulk solution. The red S-shaped curve is a fit to the data with $K_d = 350$ nM.

increasing occupancy of the originally empty receptor sites on the channel, the immobilized BSA, by the analyte anti-BSA up to a saturation level at full coverage. This is shown in figure 2(A). Upon rinsing the flow cell with pure buffer the full reversibility of the binding reaction (except for a slight drift of the device readout) suggests the applicability of a Langmuir binding model for the quantitative evaluation of both kinetic parameters for the association, k_{on}, and the dissociation constant, k_{off}, (not shown and analyzed here) and for the affinity constant, K_A, or the inverse, i.e., the dissociation constant, $K_d = 1/K_A$, equivalent to the half-saturation concentration, $c_{1/2}$ [17].

According to the Langmuir model the surface coverage, θ, is given by:

$$\theta = K_A c/(1 + K_A c). \quad (1)$$

The stationary current changes, ΔI_{SD}, reached after each change in bulk analyte concentration, c, expressed as surface coverage in percent of the full coverage, i.e.,

$$\theta = \Delta I_{SD}/\Delta I_{SD}{}^{max}, \quad (2)$$

as a function of the corresponding bulk concentration results, when plotted in a lin-log format, in the well-known S-shaped Langmuir isotherm curve. This is shown in figure 2(B). The red curve is the fit to the data with the only fitting parameter being the dissociation constant, $K_d = 350$ nM, a value well in line with reported data from the literature [27].

Immunosensing by reduced graphene oxide (rGO)-FET devices

The next example that we briefly present concerns the use of graphene as the channel material for transistor fabrication [28, 29]. In our case, for simplicity and availability of materials, we start the device fabrication with graphene oxide (GO), which upon reduction (see figure 4(A)) leads to semiconducting rGO [30]. Its excellent conductivity has one important advantage when operating in direct contact with physiological buffer solutions: even in cases where there is no protective coating that shields the electrodes or the channel material from exposure to an electrolyte with a relatively high ionic strength, the operation of the device is straightforward. The low resistance of the channel leads to a situation where 90%–95% of the current between the source and the drain electrodes passes through the rGO, and only a negligible fraction of the current runs through the electrolyte as a shortcut, which can be ignored [18]. This makes the fabrication protocol, compared to the OFET preparation described above, a lot easier as it avoids any processing steps that were essential to protect the sensitive organic/polymeric semiconducting channel material in OFETs.

Figure 3 summarizes the essential steps for the preparation of rGO–FETs, operated in the liquid-gated mode [18]. A very helpful simplification step was achieved with the use of one of the many microchips available in the electrochemical equipment market. We chose one that was only a few mm in size (figure 3(A)), and had an interdigitated Au electrode array of ~3 mm in diameter (figure 3(B)), with a spacing of 10 μm between the source and drain electrodes (figure 3(C)). The preparation of the rGO–FET, which is the conversion of this electrochemical chip into a transistor for biosensing, is given in more detail in figure 4: the electrode area is exposed to an APTES solution, a procedure which leads to the coating of the glass substrate between the Au areas with a monolayer of positive charges (figure 4(A)). These then help to attract and physisorb the GO flakes from a colloidal dispersion. Upon exposure of the deposited GO flakes to hydrazine vapor (figure 4(A)) [31] and a subsequent thermal treatment these flakes are reduced leading to highly conductive rGO flakes (bridging the space between the source and drain electrodes) [32].

The resulting conductive channels between the source and drain electrodes are randomly covered to a high degree with rGO flakes forming a continuous bridge of monomolecular or few-layer graphene sheets as was documented by AFM images (see figure 4(B) and the height scan given in figure 4(C)). The excellent conductivity was demonstrated by

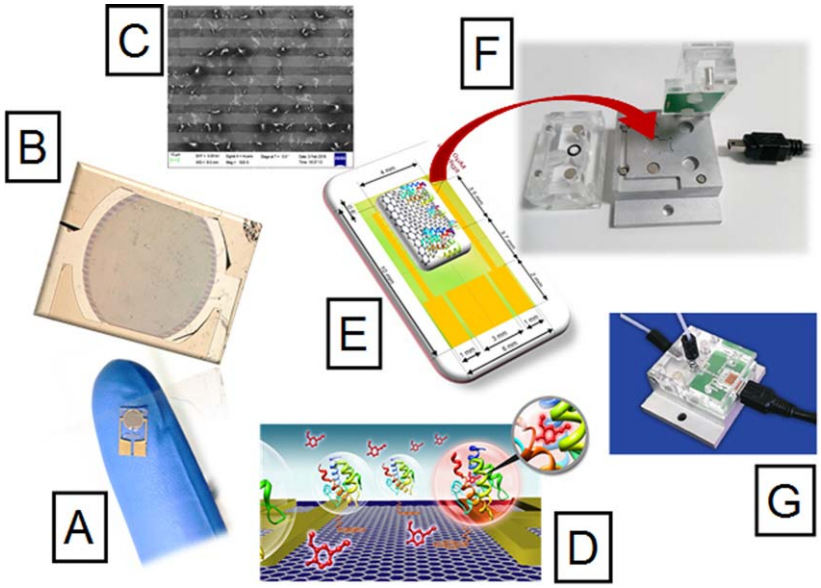

Figure 3. (A) A commercial electrochemical sensing chip on a (rubber glove-covered) fingertip. (B) Optical micrograph of the sensing area which is an interdigitated electrode array used as the source and drain electrodes. (C) A scanning electron microscope (SEM) image of the interdigitated electrode array after immobilization of graphene oxide flakes; the spacing between the electrodes is 10 μm. (D) Schematics of the immobilization of odorant binding proteins as receptors for the smell sensor via pyrene-based coupling strategies; the sensor chip (E) then fits into the commercial flow cell (F), with its analyte solution inlet and outlet and the electrical connector shown (G).

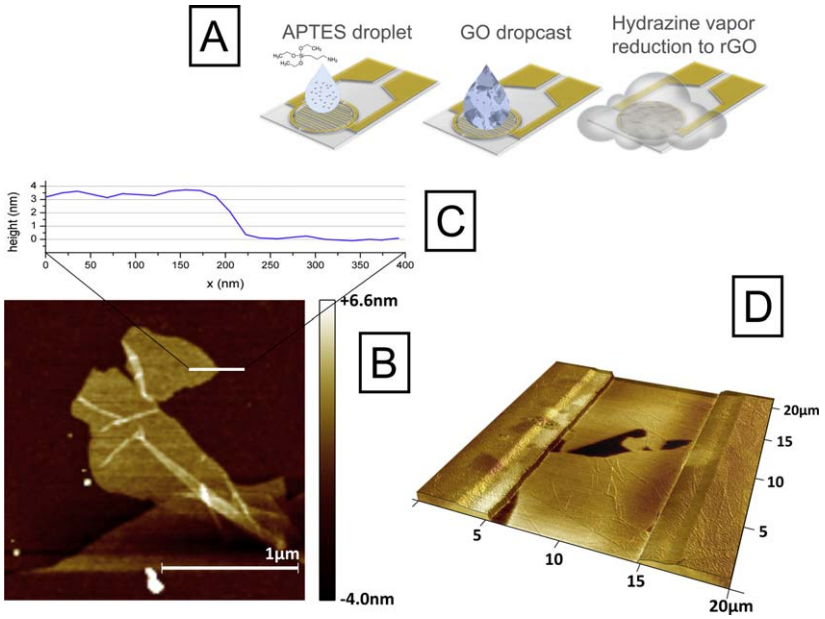

Figure 4. (A) Schematics of the chip functionalization by first covering the substrate between the Au electrodes with a monolayer of amino-propyl-triethoxy-silane (APTES), onto which the graphene oxide flaxes are deposited; after reduction by hydrazine and a thermal treatment the transistor with its semiconducting rGO flakes is ready for bio-functionalization by the receptor molecules (see also figure 3(D)). (B) Atomic force microscope (AFM) image of a single rGO flake. (C) Line scan across the edge of the rGO flake shown in (B). (D) Kelvin probe image of two Au electrodes and the space between them, covered with rGO flakes.

Kelvin probe images that were taken from the electrodes and the space between them, covered with rGO flakes (figure 4(D)). After this preparation step of coating the active area of the chip with rGO flakes (see also the SEM image given in figure 3(C)), their bio-functionalization was then conducted using a protocol borrowed from the literature describing the functionalization of carbon nanotubes [33], using 1-pyrenebutanoic acid succinimidyl ester (PBSE). The linker firmly attaches to the graphene surface through π–π interactions with the pyrene groups, and on the other end it covalently reacts with the amino group of the protein to be coupled to form an amide bond (figure 3(D)). Now the chip with its functionalized

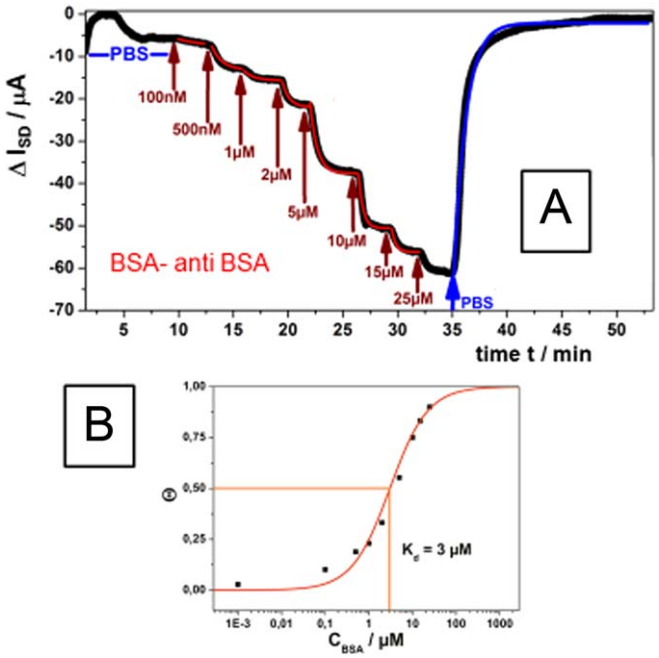

Figure 5. (A) Global analysis of BSA binding from solution to surface-immobilized anti-BSA antibody; solutions with concentrations from 100 nM to (near) saturation at 25 μM were rinsed through the flow cell. (B) Langmuir adsorption isotherm obtained by plotting the (negative) change in the source–drain current, ΔI_{SD}, scaled to its (extrapolated) maximum value, ΔI_{SD}^{max}. The red curve is a fit to the data according to the Langmuir model, resulting in a dissociation constant (half-saturation concentration) of $K_d = 3$ μM.

channel between the source and drain electrodes (figure 3(E)) is ready to be mounted into the commercial chip holder (figure 3(F)) with its convenient fluid inlet and outlet and electrical connections (figure 3(G)).

Similar to the OFET operations described above, the setup can now be used for *in situ* measurements in real time, again giving quantitative data on the reaction rate constants for the association, k_{on}, and the dissociation processes, k_{off}, as well as on the affinity constant, K_A [16].

Figure 5 presents the global analysis of the binding reaction between the surface-immobilized anti-BSA antibodies and BSA, rinsed through the flow cell at different concentrations, as indicated in figure 5(A). The red curves are fits to the association process; the blue curve is a fit to the dissociation.

The change of the source–drain current, ΔI_{SD}, measured after a new equilibrium was established, can be plotted as a function of the bulk analyte concentration to yield an adsorption isotherm, presented in figure 5(B), together with the fit to the Langmuir model with a dissociation constant of $K_d = 3$ μM.

As described by the basic equation for the electrical device performance in the liquid-gated mode of operation, i.e.,

$$I_{SD} = \mu C_{Ox} W/L(V_G - \Psi_S)V_{SD} \quad (3)$$

the source–drain current, I_{SD}, depends on the applied source–drain voltage, V_{SD}, and on the carrier mobility, μ, the gate capacity, C_{Ox}, geometric channel parameters, i.e., the width, W, and the length, L, and the Dirac voltage, V_G, determined by the threshold voltage of the cathodic branch of the hole conductance and the anodic branch of the electron conductance. Of particular importance for the device employed in electronic biosensing is the surface potential, Ψ_S, of the channel–electrolyte interface. Various contributions to the change of the current as a function of a bioaffinity reaction at the gate electrode or directly on the channel have been discussed [18, 34, 35]. The dominant contribution to the change of the surface potential upon binding of a protein to a receptor is believed to be the change in surface charge density (distribution). We demonstrated this experimentally for the electronic recording of the association and dissociation reactions of anti-BSA antibodies binding from solution to their surface-immobilized BSA antigens by changing the bulk solution pH to values below (pH 5) and above (pH 7) the pI of the analyte protein [36] which leads to an increase or a decrease of the current, corresponding to a shift of $(V_G - \Psi_S)$ to more negative or positive values, respectively [17].

Electronic biomimetic smell sensing

The interest in developing smell sensor concepts, sensors for air-born chemical analytes, odorants, pheromones, other VOCs, etc, originates from the many different potential areas where the application of such devices would be extremely relevant.

- More and more research evidence is reported in the literature that quantifies novel types of smell molecules that can be used for diagnostic purposes

[37]. For example, in a recent study the concentration of the molecule isoprene in the exhaled breath of diabetes patients could be linked to their blood glucose level [38].

- European crop losses from plant diseases amount to more than €5 billion per year [39, 40]. Plant pathogens (fungi, viruses, phytoplasma) are typically transmitted by insects using host-derived odors as key foraging cues. Thus, diseased plants draw insect vectors with specific attractant volatiles.
- Our daily protocols for testing grocery quality at home are typically based on optical inspection of the food items; what follows in most cases, however, as the ultimate quality check for edibility is a smell test.
- There is an increasing need for smell detectors in homeland security and the protection of the public and private environment: it is expected that in the future bio-inspired robots will sniff out mines, bombs, and drugs [41].

Given these few examples of the broad range of potential scenarios for the use of smell sensors, it is somewhat surprising that we have essentially no technical device worthy of the term 'artificial nose', that is able to reach the chemical bandwidth, selectivity, and sensitivity of the olfactory sense of mammals and humans or the antennae of insects. For the sensing of light, e.g. in imaging or optical communication, we have extremely powerful devices with the ability to detect even single photons. The monitoring of sound in acoustic communication is also technically unproblematic: microphones are available with an amazing performance profile. However for chemical communication, for smell or taste detection on a technical level, we have (nearly) nothing.

The attempt to detect smells by a specific kind of a chemical sensor or the development of an artificial nose is certainly not new. The general interest in artificial noses, 'electronic noses', or E-noses, originated from the many scenarios outlined above where chemical communication is extremely important in our daily life. There have been several serious attempts described in the literature to develop concepts by which, via more or less unspecific interactions of the molecules of interest (with odorants being typically small, hydrophobic molecules that are difficult to sense by classical techniques, e.g. by surface plasmon sensors with an organic (polymeric) matrix [12]), a measurable and quantifiable signal is generated. All the reported concepts, however, were eventually discarded because of the severe lack of sensitivity compared to natural olfaction.

Our approach tries to realize a biomimetic smell sensor that uses a combination of an electronic transducer, in most of our cases a rGO–FET device, and the biological functional unit used in nature by both insects and mammals, as the first recognition element

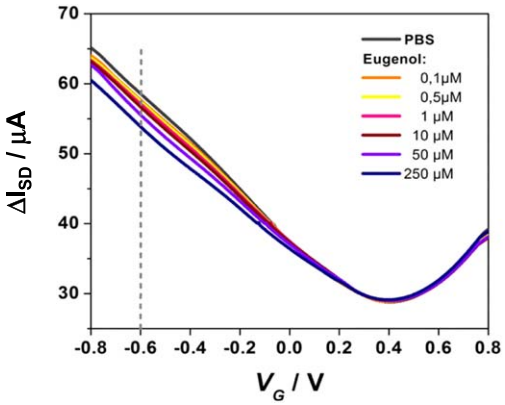

Figure 6. Current–voltage characteristics of the OBP 14 based biosensor device without eugenol, measured just in PBS, and in solutions with increasing eugenol concentrations, ranging from 100 nM to 250 μM. The applied source–drain voltage was $V_{SD} = 50$ mV.

in the smell sensing cascade, i.e., odorant binding proteins (OBPs) [42].

The preparation of the sensors follows the concepts described briefly above for immunosensors: the rGO channel is functionalized by PBSE, to which a variety of OBPs from different insects are coupled covalently by active ester chemistry [22, 43]. The chip is then integrated into the flow cell (see figure 3) and different odorant molecules in aqueous solutions of varying concentrations were then rinsed through the cell for the quantitative recording and evaluation of binding reaction rates and affinity constants for OBPs and their set of ligands.

Examples for electronic smell sensing with such a transducer are given in the following figures for a sensor that was functionalized by OBP 14 from the honey bee, *Apis mellifera*, mounted to the flow cell, and exposed to solutions of a variety of ligands.

Figure 6 gives a series of measurements of the source–drain current–gate voltage characteristics, ΔI_{SD}–V_G, for the sensor in contact with analyte solutions containing the OBP 14 ligand, eugenol, in different concentrations, ranging from pure phosphate-buffered saline solution (PBS), to a 250 μM eugenol solution. As one can see, the device performs as a bipolar FET, with the ΔI_{SD}–V_G curves affected in a quantitative way by the analyte concentration.

For a given gate voltage, in the following experiments fixed at $V_G = -600$ mV (the dashed line in figure 6) one can then use the sensor for the quantitative evaluation of the kinetic parameters of the ligand–OBP association (binding) and dissociation process, as well as, like in the case of the immunosensors described above, the binding strength, i.e. the affinity constant, K_A, of the dissociation constant K_d, respectively.

This is demonstrated in figure 7(A), which shows the global analysis, i.e. the time-dependent recordings of the change of the source–drain current, ΔI_{SD} (with the source–drain voltage set at $V_{SD} = 50$ mV and the

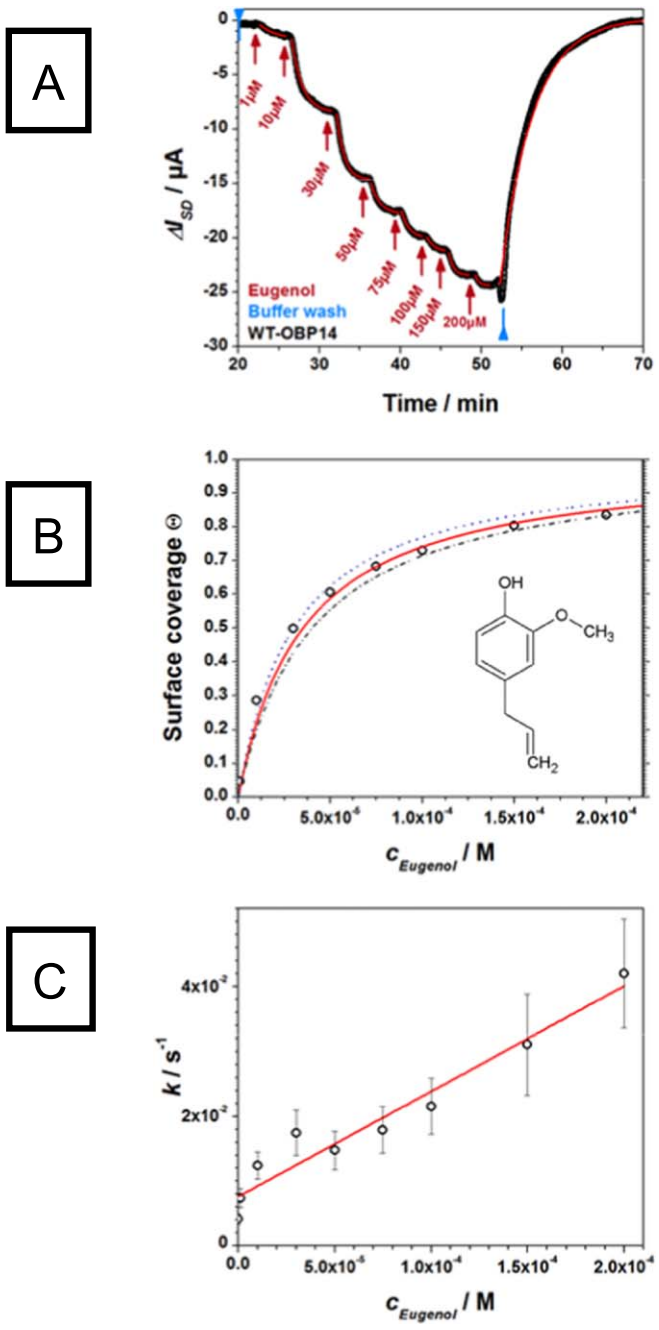

Figure 7. (A) Real time biosensor measurement (global analysis) of the binding of eugenol to OBP 14: the current decreases as the bulk concentration of eugenol increases from 1 μM to 200 μM and then saturates. Blue arrows indicate runs with pure buffer, red arrows indicate experiments with eugenol solutions. The red curves are fits to the raw data by kinetic simulations of the association and dissociation processes based on the Langmuir model. (B) Langmuir adsorption isotherm, obtained from the titration levels of (A). The red fit curve gives $K_d = 35$ μM (also plotted are error limits for K_d of $\pm 20\%$); the inset shows the structural formula of eugenol. (C) Analysis of the reaction rate constants, k, as obtained from the fitted data in (A) as a function of the eugenol concentration; error bars are $\pm 20\%$.

gate voltage at $V_G = -600$ mV, see figure 6), upon a stepwise increase of the eugenol concentration in the bulk solution until saturation of the device response is nearly reached. Upon injecting pure buffer into the flow cell again, the sensor signal returns to its baseline level showing the reversibility of the binding reaction between the ligand and its receptor immobilized on the channel of the transistor.

By plotting the respective surface coverage, θ, obtained from the equilibrium levels reached after each change of the bulk ligand concentration and scaled to the maximum response at high concentrations, see equation (2), one obtains a Langmuir adsorption isotherm from which the dissociation constant K_d can be derived. This is shown in figure 7(B): the full red curve is a fit to the data with equation (1) with $K_d = 35$ μM.

An internal consistency test for the applicability of the Langmuir model is given by the analysis of the measured association and dissociation rate constants

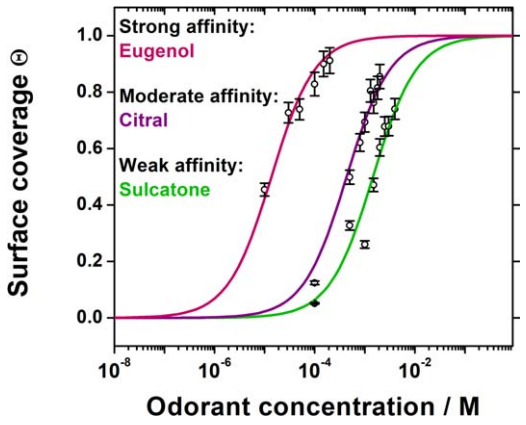

Figure 8. Langmuir adsorption isotherms for three different ligands, as indicated, for OBP 14 from *A. mellifera*.

(see the full red fit curves given in figure 7(A)). According to

$$k = k_{on}c + k_{off}, \quad (4)$$

with k_{on} being the association and k_{off} the dissociation rate constant, respectively, one obtains from the rate constants, k s^{-1}, obtained from the fits in (A) as a function of the bulk concentration, c, a straight line, as shown in figure 7(C). The slope of the fit line yields $k_{on} = 162\ M^{-1}s^{-1}$, and from the intersection of the fit line with the ordinate one obtains $k_{off} = 0.0076\ s^{-1}$. The Langmuir model predicts that the ratio k_{off}/k_{on} equals the dissociation constant, K_d, as obtained from a titration experiment. From the data in figure 7(C) we obtain $K_d = 47\ \mu M$, which agrees very well with the value from figure 7(B), i.e., $K_d = 35\ \mu M$.

Finally, we present some examples for the selective response of such an electronic smell sensor based on OBP functionalized rGO–FETs to different ligands. The sensor used for the experiments given in figure 8 had OBP 14 from *A. mellifera* immobilized on its channel and it was exposed to a variety of different analyte solutions. The odorants bind to the identical receptor with affinity constants that differ by more than two orders of magnitude in their binding strength. The full range that we found for a set of 14 different ligands even covered even three orders of magnitude [43]. Moreover, the sequence of strong and weak affinity ligands qualitatively matches a set of data obtained from a fluorescence assay in solution. A comprehensive comparison of data from receptors immobilised onto a rGO–FET with a fluorescence displacement assay in solution is currently in progress in our laboratory.

Concusions

Electronic biosensing shows great promise for complementing electrochemical detection schemes on the one hand and optical concepts for the quantitative monitoring of bioanalytes on the other. In particular, the use of graphene as the conductive gate material in the preparation of thin film transistors as sensing devices offers a tremendous advantage compared to the use of organic semiconducting materials or compared to Si-based transistors, which both require far more demanding preparation protocols. This has been demonstrated convincingly in many examples reported in the literature. With the introduction of graphene as the semiconducting material used for the fabrication of a channel of a water-stable transistor [10] the electronic read-out concept has become even more attractive.

The use of antibodies as receptors for protein and peptide markers and of odorant binding proteins in smell sensors will be complemented by the development of artificial receptors, e.g. aptamers [44], affimers [45], or seligos [46]. Immunodiagnostics with graphene FETs functionalized by these synthetic immunoreceptors for proteins, but also for the detection of small analytes, are just beginning a very dynamic development in biosensing. All of these electronic biosensing platforms are highly sensitive, label-free, disposable and cheap, with signals that are easy to analyze and interpret, suitable for multiplexed operation and for remote control, compatible with NFC technology, etc, and are in many cases a clear and promising alternative to optical sensors.

Acknowledgments

Partial support for this work was provided by the European Science Foundation (ESF), grant number 10-EuroBioSAS-FP-005, the Austrian Science Fund (FWF) (I681-N24), the Austrian Federal Ministry for Transportation, Innovation and Technology (GZBMVIT-612.166/0001-III/I1/2010), by the FFG within the Comet Program, and from the governments of Lower and Upper Austria.

ORCID iDs

Caroline Kotlowski https://orcid.org/0000-0001-5416-5837
Wolfgang Knoll https://orcid.org/0000-0003-1543-4090

References

[1] Shen G and Fan Z (ed) 2016 *Flexible Electronics, From Materials to Devices* (Singapore: World Scientific)
[2] Lipomi D J and Bao Z 2017 Stretchable and ultraflexible organic electronics *MRS Bull.* **42** 93–7
[3] Myers A, Bowles A, Shahariar H, Bhakta R and Jesse S J 2017 *Wearable Electronics* (Marietta, GA: Textile World)
[4] Han T-H, Kim H, Kwon S-J and Lee T-W 2017 Graphene-based flexible electronic devices *Mater. Sci. Eng.* R **118** 1–43
[5] Lipomi D J, Vosgueritchian M, Tee B C-K, Hellstrom S L, Lee J A, Fox C H and Bao Z 2011 Skin-like pressure and strain

sensors based on transparent elastic films of carbon nanotubes *Nat. Nanotechnol.* **6** 788–92
[6] Frazier K M and Swager T M 2013 Robust cyclohexanone selective chemiresistors based on single-walled carbon nanotubes *Anal. Chem.* **85** 7154–8
[7] Meredith S E, Robinson A, Erb P, Spieler C A, Klugman N, Dutta P and Dallery J 2014 A mobile-phone-based breath carbon monoxide meter to detect cigarette smoking *Nicotine Tob. Res.* **16** 766–73
[8] Stoppa M and Chiolerio A 2014 Wearable electronics and smart textiles: a critical review *Sensors* **14** 11957–92
[9] Bazaka K and Jacob M V 2013 Implantable devices: issues and challenges *Electronics* **2** 1–34
[10] Liao C, Mak C, Zhang M, Chan H L and Yan F 2015 Flexible organic electrochemical transistors for highly selective enzyme biosensors and used for saliva testing *Adv. Mater.* **27** 676–81
[11] Roberts M E, Mannsfeld S C B, Queraltó N, Reese C, Locklin J, Knoll W and Bao Z 2008 Water-stable organic transistors and their application in chemical and biological sensors *Proc. Natl Acad. Sci.* **105** 12134–9
[12] Crone B, Dodabalapur A, Gelperin A, Torsi L, Katz H E, Lovinger A J and Bao Z 2001 Electronic sensing of vapors with organic transistors *Appl. Phys. Lett.* **78** 2229–31
[13] Diacci C, Berto M, Lauro M D, Bianchini E, Pinti M, Simon D T, Biscarini F and Bortolotti C A 2017 Label-free detection of interleukin-6 using electrolyte gated organic field effect transistors *Biointerphases* **12** 05F401
[14] Khan H U, Roberts M E, Knoll W and Bao Z 2011 Pentacene based organic thin film transistors as the transducer for biochemical sensing in aqueous media *Chem. Mat.* **23** 1946–53
[15] Lai S, Viola F A, Cosseddu P and Bonfiglio A 2018 Floating gate, organic field-effect transistor-based sensors towards biomedical applications fabricated with large-area processes over flexible substrates *Sensors* **18** 688
[16] Reiner-Rozman C, Kotlowski C and Knoll W 2015 Electronic biosensing with functionalized rGO FETs *Biosensors* **6** 17
[17] Khan H U, Jang J, Kim J J and Knoll W 2011 *In situ* antibody detection and charge discrimination using aqueous stable pentacene transistor biosensors *J. Am. Chem. Soc.* **133** 2170–6
[18] Reiner-Rozman C, Larisika M, Nowak C and Knoll W 2016 Graphene-based liquid-gated field effect transistor for biosensing: theory and experiments *Biosensors Bioelectron.* **70** 21–7
[19] Khan H U, Roberts M E, Johnson O, Förch R, Knoll W and Bao Z 2010 *In situ*, label-free DNA detection using organic transistor sensors *Adv. Mater.* **22** 4452–6
[20] Berto M *et al* 2018 EGOFET peptide aptasensor for label-free detection of inflammatory cytokines in complex fluids *Adv. Biosyst.* **2** 1700072
[21] Aspermair P, Szunerits S and Knoll W in preparation
[22] Larisika M *et al* 2015 Electronic olfactory sensor based on *A. mellifera* odorant-binding protein 14 on a reduced graphene oxide field-effect transistor *Angewandte Chemie* **127** 13443–6
[23] Gianelli M, Roskamp R F, Jonas U, Loppinet B, Fytas G and Knoll W 2008 Dynamics of swollen gel layers anchorred to solid surfaces *Soft Matter* **4** 1443–7
[24] Fromherz P, Offenhäusser A, Vetter T and Weis J 1991 A neuron-silicon-junction: a Retzius-cell of the leech on an insulated-gate field-effect transistor *Science* **252** 1290–3
[25] Lauer L, Vogt A, Yeung C K, Knoll W and Offenhäusser A 2002 Electrophysiological recordings of patterned rat brain stem slice neurons *Biomaterials* **23** 3123–30
[26] Roberts M E, Queralto N, Mannsfeld S C B, Reinecke B N, Knoll W and Bao Z 2009 Cross-linked polymer gate dielectric films for low-voltage organic transistors *Chem. Mat.* **21** 2292–9
[27] Olson W C, Spitznagel T M and Yarmush M L 1989 Dissociation kinetics of antigen-antibody interactions: studies on a panel of anti-albumin monoclonal antibodies *Mol. Immunol.* **26** 129–36
[28] Schwierz F 2010 Graphene transistors *Nat. Nanotechnol.* **5** 487–96
[29] Lee S-K, Kim B J, Jang H, Yoon S C, Lee C, Hong B H, Rogers J A, Cho J H and Ahn J-H 2011 Stretchable graphene transistors with printed dielectrics and gate electrodes *Nano Lett.* **11** 4642–6
[30] Hummers Jr, William S and Offeman R E 1958 Preparation of graphitic oxide *J. Am. Chem. Soc.* **80** 1339
[31] Larisika M, Huang J F, Tok A, Knoll W and Nowak C 2012 An improved synthesis route to graphene for molecular sensor applications *Mater. Chem. Phys.* **136** 304–8
[32] Bintinger J, Eder D and Knoll W in preparation
[33] Georgakilas V, Kordatos K, Prato M, Guldi D M, Holzinger M and Hirsch A 2002 Organic functionalization of carbon nanotubes *J. Am. Chem. Soc.* **124** 760–1
[34] Melzer K, Brändlein M, Popescu B, Popescu D, Lugli P and Scarpa G 2014 Characterization and simulation of electrolyte-gated organic field-effect transistors *Faraday Discuss.* **174** 399–411
[35] Knopfmacher O, Tarasov A, Fu W, Wipf M, Niesen B, Calame M and Schönenberger C 2010 Nernst limit in dual-gated Si-nanowire FET sensors *Nano Lett.* **10** 2268–74
[36] Chun K-Y and Stroeve P 2002 Protein transport in nanoporous membranes modified with self-assembled monolayers of functionalized thiols *Langmuir* **18** 4653–8
[37] Nakhleh M K *et al* 2017 Diagnosis and classification of 17 diseases from 1404 subjects via pattern analysis of exhaled molecules *ACS Nano* **11** 112–25
[38] Neupane S, Peverall R, Richmond G, Blaikie T P, Taylor D, Hancock G and Evans M L 2016 Exhaled breath isoprene rises during hypoglycemia in type 1 diabetes *Diabetes Care* **39** e97–8
[39] Oerke E-C 2006 Crop losses to pests *J. Agric. Sci.* **144** 31–43
[40] Nelson A D, Savary S, Willocquet L, Esker P, Pethybridge S J and McRoberts N 2018 Assessment of crop health and losses to plant diseases in world agricultural foci *Int. Congress of Plant Pathology 2018: Plant Health in a Global Economy*
[41] Bromenshenk J J, Henderson B B, Seccomb R A, Welch P M, Debnam S E and Firth D R 2015 Bees as biosensors: chemosensory ability, honey bee monitoring systems, and emergent sensor technologies derived from the pollinator syndrome *Biosensors* **5** 678–711
[42] Pelosi P, Mastrogiacomo R, Iovinella I, Tuccori E and Persaud K C 2014 Structure and biotechnological applications of odorant-binding proteins *Appl. Microbiol. Biotechnol.* **98** 61–70
[43] Kotlowski C, Larisika M, Guerin M, Kleber C, Kröber T, Mastrogiacomo R, Nowak C, Pelosi P, Schwaighofer A and Knoll W 2018 Fine discrimination of volatile compounds by graphene-immobilized odorant-binding proteins *Sensors Actuators* B **256** 564–72
[44] Bruno J G 2015 Predicting the uncertain future of aptamer-based diagnostics and therapeutics *Molecules* **20** 6866–87
[45] Tiede C 2017 Affimer proteins are versatile and renewable affinity reagents *eLife* **6** e24903
[46] Jur J, Bowles A, Bhakta R, Mayers A, Shahariar H and Twiddy J 2017 Design and commercialization challenges of garment-based textile electronics *The Electrochemical Society Meeting Abstracts* (vol 50) pp 2121